Scattering-assisted electric current in semiconductor superlattices in the Wannier-Stark regime

Yu. A. Tarakanov,[1] V. Vettchinkina,[2] M. A. Odnoblyudov,[1] K. A. Chao,[2] N. Sekine,[3] and K. Hirakawa[3]
[1]*A. F. Ioffe Physico-Technical Institute, Russian Academy of Science, 194021 St. Petersburg, Russia*
[2]*Division of Solid State Theory, Department of Physics, Lund University, S-223 62 Lund, Sweden*
[3]*Institute of Industrial Sciences, University of Tokyo, Tokyo, Japan*
(Received 19 May 2005; revised manuscript received 8 August 2005; published 30 September 2005)

We have used the Monte Carlo technique to investigate the mechanism of scattering-assisted charge transport in semiconductor superlattices under a strong applied electric field in the Wannier-Stark (WS) regime. The distribution function of quasi-two-dimensional carriers localized in each WS level is calculated, and the contributions of different scattering mechanisms to the total scattering probability are analyzed. Based on these results, the drift velocity is derived as a function of the applied electric field. Due to the LO-phonon-induced resonant transfer of electrons between different spatially localized WS states, our calculated *I-V* characteristics oscillates with clear negative differential velocity behavior. At the electric field strength such that the Bloch oscillation energy is equal to an integer multiple of the LO phonon energy, a peak appears in the *I-V* curve. Our theoretical result agrees with the experimental data which was obtained from analyzing the terahertz response of superlattices to picosecond optical pulse excitation.

DOI: 10.1103/PhysRevB.72.125345 PACS number(s): 73.21.Fg, 73.20.Hb

I. INTRODUCTION

The dynamics of Bloch electrons under a strong dc electric field has been a much studied subject but not completely understood. The availability of high-quality semiconductor superlattices (SSLs) with controllable lattice periodicity d has stimulated extensive investigation on various interesting relevant phenomena. With an electric field $\mathcal{E}$ applied perpendicular to the interfaces, the electron transport is characteristic to the one-dimensional minibands of a superlattice. Esaki and Tsu[1] pointed out that in such a system the electrons can demonstrate a negative differential drift velocity with increasing $\mathcal{E}$. They also proposed to make use of this nonlinear transport property to generate electromagnetic radiation.

We assign the z axis for the growth direction of the SSL, and the xy plane parallel to the interfaces. In the absence of an external electric field, in the SSL the total electron energy $\varepsilon_{tot}=\varepsilon_{\mathbf{k}_\parallel}+E_n(k_z)$ contains the two-dimensional electron gas energy $\varepsilon_{\mathbf{k}_\parallel}=\hbar^2(k_x^2+k_y^2)/(2m)$ with an effective mass m, and the miniband energy $E_n(k_z)$. Except for the case of extremely strong electric field which causes Zener tunneling between two minibands, it is sufficient to consider only one miniband to study the dynamics of Bloch electrons. This is the situation to be treated here in our work.

When an external electric field $\mathcal{E}$ is applied along the z axis, in quasiclassical approximation the time evolution of the electron wave vector component k_z is given by $k_z(t)=e\mathcal{E}t/\hbar$, where e is the electron charge. If an electron does not suffer any scattering, because of the Bragg reflection at the Brillouin-zone boundaries $k_z=\pm\pi/d$, it oscillates in k_z space with a Bloch-oscillation (BO) frequency $\omega_B=ed\mathcal{E}/\hbar$. The corresponding electron motion in real space is also an oscillation with the same BO frequency ω_B.

In reality the electron is scattered with a relaxation time τ. Within a time interval τ the electron performs the above described quasiclassical oscillation in both k space and real space. We can define a threshold field $\mathcal{E}_0=\hbar/ed\tau$ under which the BO frequency satisfies the condition $\omega_B\tau=1$. For a weak field $\mathcal{E}<\mathcal{E}_0$, the electron cannot complete even one cycle of BO before being scattered, and hence its transport properties can be described in terms of a drift velocity. This drift velocity increases with the electric field strength. In the high-field limit $\omega_B\tau\gg1$, an electron can perform many cycles of BO without suffering a scattering. In this case the Bloch electrons can hardly contribute to the net charge transport, and consequently the drift velocity of electrons in a SSL approaches zero. As a result, the negative differential drift velocity appears in the high-field regime $\mathcal{E}\gg\mathcal{E}_0$.

In a bulk crystal the lattice constant is so small that the corresponding threshold field $\mathcal{E}_0$ is too high to be achieved in reality. The large value of the periodicity d in SSL samples provides the possibility to observe the BO and related physical properties. Many experiments[2–6] have indeed confirmed the existence of BO in SSL at low temperatures as well as at room temperatures. Shortly after the proposal of Esaki and Tsu,[1] there appeared a theoretical study[7] on the interaction between a weak field of terahertz (THz) frequency ω and the electrons in a SSL miniband performing BO with allowed energy relaxation. It was suggested that such an interaction can lead to an amplification of the THz field in the region of ω less than the BO frequency ω_B, and the amplification curve exhibits a resonancelike structure around $\omega\simeq\omega_B$.

An extension of the weak-field theory[7] of amplification to the case of a strong THz field[8–10] indicated the possible resonant amplification of THz fields at $\omega=n\omega_B$ with integer n. According to a recent theoretical analysis[11] this type of amplification of THz radiation is associated to k-space electron bunching. The amplification of THz radiation was studied with one-dimensional models[8–10] as well as using Green's functions[12] and three-dimensional Monte Carlo approaches.[13,14] In the paper by Schomburg *et al.*[14] it was demonstrated that in the framework of a miniband description, the bunching is mainly mediated by the spontaneous phonon emission by the Bloch oscillating electrons.

With increasing strength of $\mathcal{E}$, the quasiclassical method becomes less reliable and one needs a full quantum mechanical approach. The analytical solution of Wannier[15] proves that the energy spectrum of a Bloch electron under an external dc field $\mathcal{E}$ consists of an infinite series of eigenvalues which are equally separated by an energy difference $e\mathcal{E}d = \hbar\omega_B$. This series of eigenenergies is called the Wannier-Stark ladder (WSL). The corresponding eigenfunctions are also equally displaced by a distance d in real space along the field direction. The time-domain analog to the WSL is the periodic motion of an electron along its dispersion $E_n(k_z)$ in k_z space, or the spatial BO of an electron in real space.

In a realistic SSL sample, the levels in a WSL are broadened by scatterings. Under a weak field $\mathcal{E}$, the small energy separation $e\mathcal{E}d$ is smeared out by scatterings, and so the quasiclassical energy band description is a good approximation. When the field strength increases and becomes larger than $\mathcal{E}_0$, the WSL levels become well resolved and electron eigenfunctions in the SSL tend to be localized at the superlattice sites. It is important to notice that the same threshold field $\mathcal{E}_0$ appears for both the formation of the WSL and the occurrence of the negative differential drift velocity, or the negative differential conductance. This suggests strongly that the NDC of a SSL originates from WSL-type localization of the electron wave functions. In this situation the dynamical processes to generate a current flow in the SSL are the scattering-assisted transitions between different WSL levels.

The hopping conduction in a superlattice due to transitions of carriers between WSL mediated by interaction with acoustic phonons was studied by Tsu and Döhler.[16] They demonstrated that negative differential conductance may occur in this case. The current-voltage characteristic was calculated under the assumption that hopping events do not change the in-plane equilibrium distribution of quasi-two-dimensional carriers with respect to the parallel momentum components k_x and k_y. In the later study by Bryksin and Kleinert,[17] the hopping current due to interaction with polar optical phonons was considered. The in-plane distribution function was determined as a solution to quantum kinetic equation and was shown to deviate significantly from the equilibrium one. While the calculations show the presence of resonant-type current peaks associated with the electron-phonon resonances; however, both elastic alloy disorder and acoustic phonon scattering, which may significantly affect the distribution function, have not been taken into account.

In our present paper, the electron transport in SSL under an applied dc electric field, driven by the scattering-assisted electron transitions between neighboring WSL levels, is studied with a Monte Carlo approach. To provide a complete picture of the physical phenomenon, we investigate the combined effect of optical phonon scattering, acoustic phonon scattering, and elastic alloy disorder scattering. We analyze the contribution of each scattering mechanism to the total current, as well as effect of each scattering mechanism on the carrier distribution function. Our calculated field dependence of the drift velocity will be compared with the data obtained recently from the experiments on time-domain THz spectroscopy of an AlGaAs/GaAs SL.[18] These experiments provide a method to determine the electric field dependence of the drift velocity of carriers in undoped SSL.

II. WSL STATES IN A BIASED SSL

To study the scattering-assisted electron transport between WSL levels in a SSL under an external dc field, in order to reach high quantitative accuracy, we must use the electron eigensolutions to calculate the matrix elements of all scattering processes. If the electric field $\mathcal{E}$ is not extremely strong so as to cause Zener tunneling, the eigensolutions of the WSL levels can be derive with a well-established computation scheme.[19] Here we will only outline the computation procedure.

Since the field $\mathcal{E}$ is applied along the z axis parallel to the growth direction, in the effective mass approximation the wave functions in the xy plane are simply plane waves with the corresponding eigenenergies $\varepsilon_{k_\parallel} = \hbar^2(k_x^2 + k_y^2)/(2m)$. The total wave function $\Psi_{i\mathbf{k}_\parallel}(\mathbf{r})$ can be expressed as

$$\Psi_{i\mathbf{k}_\parallel}(\mathbf{r}) = \frac{\exp i(k_x x + k_y y)}{\sqrt{S}} \psi_i(z), \tag{1}$$

where S is the normalization area. The wave function $\psi_i(z)$ and the corresponding eigenenergy E_z^i, which describe the WSL, must be derived from the Schrödinger equation

$$\left(-\frac{\hbar^2}{2} \frac{\partial}{\partial z} \frac{1}{m} \frac{\partial}{\partial z} + V(z) + e\mathcal{E}z \right) \psi_i(z) = E_z^i \psi_i(z). \tag{2}$$

Since the samples used in experiments are of finite length, the potential function $V(z)$ in the above equation should be a multiple-period square-well potential, bounded at each end by a higher potential barrier simulating the work function.

We will solve Eq. (2) by expanding $\psi_i(z)$ in terms of a complete set of basis functions. Let us first consider a SSL of infinitive length in the absence of the electric field, $\mathcal{E}=0$. The Bloch states of each miniband in this SSL can be derived easily. Since the Zener tunneling will not appear in the system to be studied here, we will treat individual subbands separately. From the Bloch states of a given miniband, we can construct the complete set of Wannier functions $a(z-nd)$, where i runs over all integers. Then, we expresses the wave function $\psi_i(z)$ as

$$\psi_i(z) = \sum_n f_i^n a(z - nd). \tag{3}$$

The coefficients of expansion f_i^n and the corresponding energy E_z^i for a SSL sample of finite size can be obtained easily via matrix diagonalization. The detailed computation procedure can be found in Ref. 19. These eigenfunctions in the WSL are spatially equally separated by the lattice constant d, in agreement with the theoretical predication of Wannier.[15] To avoid any ambiguity in our future description, we will enumerate our eigensolutions according to their spatial location, and use the terminology that the eigenstate $\psi_i(z)$ is localized in the ith unit cell of the SSL sample. The total energy of the electron in the SSL is then

$$E_{i\mathbf{k}_\parallel} = E_z^i + \varepsilon_{k_\parallel}. \tag{4}$$

The experiment to which we will compare our calculated results is performed on an $Al_{0.3}Ga_{0.7}As/GaAs$ SSL with 73 periods. The GaAs well width is $d_w = 6.5$ nm and the

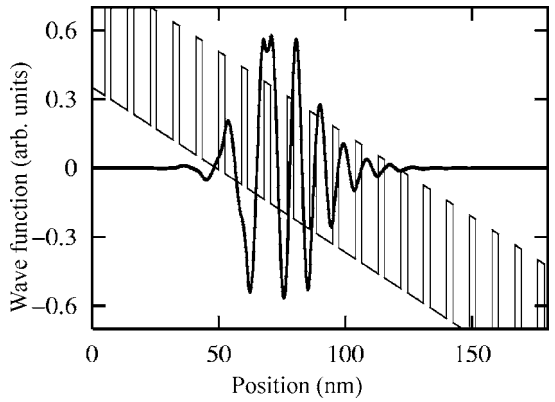

FIG. 1. The wave function corresponding to a WS level under an electric field of 36 kV/cm. The potential profile is plotted in dashed lines.

$Al_{0.3}Ga_{0.7}As$ barrier width is $d_b=2.5$ nm. One eigenfunction $\psi_i(z)$ in the WSL together with the total potential function $V(z)+e\mathcal{E}z$ are plotted in Fig. 1 for a field strength $\mathcal{E}=36$ kV/cm.

III. SCATTERING-ASSISTED TRANSPORT THROUGH A WSL

We will investigate the carrier transport along the SSL growth direction for the electric field strength $\mathcal{E}$ stronger than the threshold field $\mathcal{E}_0$. In this case the semiclassical theory is no longer valid and carrier transport occurs via scattering-assisted hops between the WSL states $\psi_i(z)$ localized in different SSL unit cells. In a GaAs/AlGaAs SSL the essential scattering mechanisms are the alloy disorder scattering, the polar optical phonon scattering, and the acoustic scattering due to both the deformation potential and the piezoelectric interaction.

The scattering-assisted carrier hopping is illustrated schematically in Fig. 2, where the positions of the unit cells in the SSL are marked as $i-1, i, i+1, i+2, \ldots$. The WSL levels E_z^i are attached to these unit cells as indicated by horizontal lines, together with a series of two-dimensional energy dispersions $\varepsilon_{\mathbf{k}_\parallel}$. We notice that the WSL levels E_z^i are equally separated by the BO energy $\hbar\omega_B$.

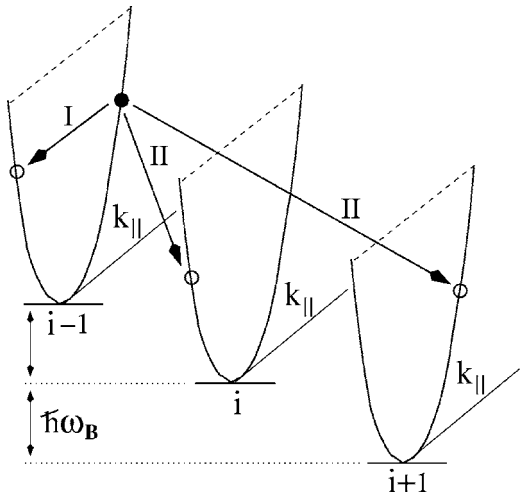

FIG. 2. A schematic illustration of the scattering-induced hopping transport in a biased SSL in the WSL regime.

A carrier that occupies its initial state $\Psi_{i\mathbf{k}_\parallel}(\mathbf{r})$ marked by the solid dot in Fig. 2 can either be scattered into the states at the same WSL energy level E_z^i (this *intralevel* scattering is indicated in Fig. 2 as process I), or it can hop to the state $\Psi_{j\mathbf{k}_\parallel'}(\mathbf{r})$ associated with another WSL energy level E_z^j, with $j\neq i$ (this *interlevel* scattering is indicated in Fig. 2 as process II). The intralevel scattering cannot produce a finite current, but can significantly affect the distribution function over the two-dimensional momentum $\mathbf{k}_\parallel$. In the presence of a strong electric field, the electron system in a SSL can be viewed as a number of quasi-two-dimensional electron ensembles, each of which is localized in one SSL unit cell. These ensembles are coupled by the *interlevel* scattering mechanisms to be introduced below.

The hopping of electrons can occur via the emission or absorption of phonons as well as by elastic alloy disorder scattering. The rates of various scattering processes between $\Psi_{i\mathbf{k}_\parallel}(\mathbf{r})$ and $\Psi_{j\mathbf{k}_\parallel'}(\mathbf{r})$ depend on the applied field strength and the temperature. As an example to clarify this point, let us assume a small momentum component $\mathbf{k}_\parallel$ of the electron in its initial state $\Psi_{i\mathbf{k}_\parallel}(\mathbf{r})$ such that the associated kinetic energy $\varepsilon_{k_\parallel}$ is less than the BO energy $\hbar\omega_B$. This is usually the situation if the applied electric field is strong and the temperature is not too high. Via the emission of phonons or by elastic scattering the electron can hop to the state $\Psi_{j\mathbf{k}_\parallel'}(\mathbf{r})$ only if $j>i$. Such interlevel scattering processes are marked in Fig. 2 as process I. Interlevel scattering via the absorption of phonons can be significant only at high temperatures. Interlevel scattering will produce a drift electric current flowing through the SSL. In our numerical calculations of this current, all interlevel scattering-assisted transport processes are included.

We would like to point out that a similar mechanism of scattering-assisted hops between unit cells in a disordered SSL in the absence of an external electric field has been studied.[20] However, since there is no electric driving force, the electron transport has the character of diffusion rather than drift, and there is no net current flow.

It is important to emphasize here that in our study the electric field strength is not extremely high so as to cause Zener tunneling. Hence, the scattering-assisted hops are restricted within the WSL associated with one miniband. In the following we will derive the scattering rates of optical phonon, acoustic phonon, and alloy disorder.

For the convenience of presentation, we will use the braket notation to represent the electron state $\Psi_{i\mathbf{k}_\parallel}(\mathbf{r})$ by $|i\mathbf{k}_\parallel\rangle$. We will first treat the scattering of electrons by a three-dimensional phonon with momentum $\mathbf{q}$. Let $\omega_\mathbf{q}$ be the phonon dispersion and $C(\mathbf{q})$ the electron-phonon coupling function. Following the Fermi golden rule, the rate of the phonon-assisted transitions between the state $|i\mathbf{k}_\parallel\rangle$ and the state $|i'\mathbf{k}_\parallel'\rangle$ has the form

$$W^{PH}_{i\mathbf{k}_\parallel,i'\mathbf{k}'_\parallel} = \frac{2\pi}{\hbar}\sum_{\mathbf{q}} |C(\mathbf{q})|^2 \langle i\mathbf{k}|\exp(i\mathbf{q}\cdot\mathbf{r})|i'\mathbf{k}'\rangle^2 \times [N_{\mathbf{q}}\delta(E_{i\mathbf{k}_\parallel} - E_{i'\mathbf{k}'_\parallel} + \hbar\omega_{\mathbf{q}}) + (N_{\mathbf{q}}+1)\delta(E_{i\mathbf{k}_\parallel} - E_{i'\mathbf{k}'_\parallel} - \hbar\omega_{\mathbf{q}})], \quad (5)$$

where $N_{\mathbf{q}} = 1/[\exp(\hbar\omega_{\mathbf{q}}/k_BT) - 1]$ is the number of phonons with wave vector $\mathbf{q}$ at temperature T.

The coupling function $|C(\mathbf{q})|^2$ of electrons to phonons in zinc-blende semiconductor structures was derived[20] as

$$|C(\mathbf{q})|^2_{OPP} = \frac{2\pi e^2}{V}\left(\frac{1}{\epsilon_\infty} - \frac{1}{\epsilon_0}\right)\frac{\hbar\omega_{\mathbf{q}}}{q^2} \quad (6)$$

for polar coupling to optical phonons (OPP),

$$|C(\mathbf{q})|^2_{APD} = \frac{D^2\hbar}{2V\rho C_s}q \quad (7)$$

for deformation-potential coupling to acoustic phonons (APD), and

$$|C(\mathbf{q})|^2_{APP} = \frac{8\pi^2 e^2\hbar P^2}{V\epsilon^2_\infty\rho}\frac{K_h^2}{\omega_{\mathbf{q}}} \quad (8)$$

for piezoelectric coupling to acoustic phonons (APP). In the above equations, V is the volume of the system, ρ the mass density, D the deformation potential constant, C_s the sound velocity, ϵ_∞ the electronic dielectric constant, and ϵ_0 the the total dielectric constant including the ionic screening. The piezoelectric constant P can be expressed in terms of the third-rank piezoelectric tensor elements as $P = 2e_{123} = 2e_{14}$, and $K_h \equiv \hat{q}_1\hat{p}_2\hat{p}_3 + \hat{q}_2\hat{p}_1\hat{p}_3 + \hat{q}_3\hat{p}_1\hat{p}_2$ in terms of the components $\hat{q}_i$ of the unit momentum vector $\hat{\mathbf{q}}$ and the components $\hat{p}_i$ of the polarization vector $\hat{\mathbf{p}}$.

In our numerical calculation, we use the commonly accepted approximation $\omega_{\mathbf{q}} = C_{sq}$ for acoustic phonons and $\omega_{\mathbf{q}} = \omega_{LO}$ for optical phonons. For the polar coupling to optical phonons and the deformation-potential coupling to acoustic phonons, we only retain the dominating longitudinal mode. However, all polarization modes contribute to the piezoelectric coupling between electrons and acoustic phonons. For this case, we follow Ref. 20 to approximate K_h^2 by its average $\tilde{K}_h^2$ over the direction of $\hat{\mathbf{q}}$:

$$\tilde{K}_h^2 = \frac{9}{8}\sin^4\theta\cos^2\theta + \frac{1}{2}\cos^2\theta\sin^2\theta + \frac{1}{8}(3\cos^2\theta - 1)^2\sin^2\theta, \quad (9)$$

where θ is the angle between $\mathbf{k}$ and $\mathbf{k}'$. In the above equation, at the right-hand side, the first term is due to the longitudinal mode, and the other two terms are due to the transverse modes.

There have been a number of theoretical studies on electron scattered by alloy disorder potential.[21] The scattering rate can be generally expressed as

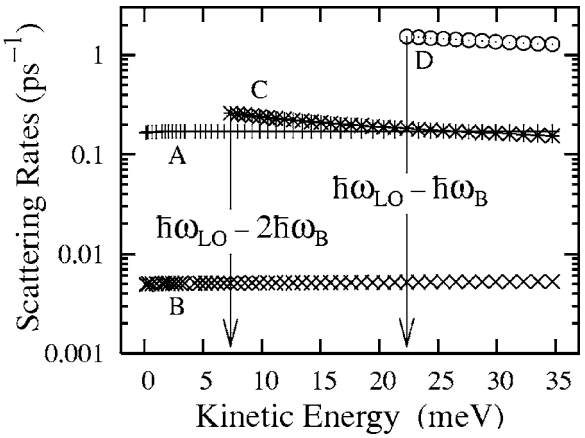

FIG. 3. The calculated scattering rates $P^I_{i\mathbf{k}_\parallel}$ as functions of the kinetic energy $\varepsilon_{\mathbf{k}_\parallel}$: curve *A* for the alloy disorder scattering, curve *B* for the acoustic phonon scattering due to deformation potential and piezoelectric interaction, curves *C* and *D* for the LO phonon emission processes from $|i,\mathbf{k}\rangle$ to $|i+1,\mathbf{k}'\rangle$ and to $|i+2,\mathbf{k}'\rangle$, respectively.

$$W^{AD}_{i\mathbf{k}_\parallel,i'\mathbf{k}'_\parallel} = \frac{2\pi}{\hbar}|M(i\mathbf{k}_\parallel, i'\mathbf{k}'_\parallel)|^2\delta(E_{i\mathbf{k}_\parallel} - E_{i'\mathbf{k}'_\parallel}). \quad (10)$$

We model the alloy disorder potential with a set of randomly distributed scattering centers, and the potential at each scattering center is a spherical well of height ΔE and radius r_0. Then the scattering matrix elements in a ternary alloy $A_xB_{1-x}C$ were derived as[21]

$$|M(i\mathbf{k}_\parallel, i'\mathbf{k}'_\parallel)|^2 = (4\pi r_0^3\Delta E/3)^2\frac{L}{V}N_0x(1-x) \times \sum_{\mathbf{q}_\parallel}\delta(\mathbf{k}'_\parallel, \mathbf{k}_\parallel + \mathbf{q}_\parallel)\int dz|\psi_i(z)\psi_{i'}(z)|^2, \quad (11)$$

where N_0 is the number of scattering centers per unit volume.

We will demonstrate the characteristic features of the scattering rate with our calculated result using a $GaAs/Al_{0.3}Ga_{0.7}As$ SSL sample under an applied electric field 16 kV/cm. For this field strength the BO energy is 14.4 meV. We use the reasonable parameter values $\Delta E = 0.6$ eV, $r_0 = 2.5$ Å, and $N_0 = 6.6\times10^{21}$ cm^{-3} in our numerical calculation. For a given initial state $|i\mathbf{k}_\parallel\rangle$ we calculate $W^{AD}_{i\mathbf{k}_\parallel,i'\mathbf{k}'_\parallel}$ for alloy disorder scattering and $W^{PH}_{i\mathbf{k}_\parallel,i'\mathbf{k}'_\parallel}$ for all types of phonon scattering. Then, the rate for removing an electron from the initial state $|i\mathbf{k}_\parallel\rangle$ due to the *I*th scattering mechanism is

$$P^I_{i\mathbf{k}_\parallel} = \sum_{i',\mathbf{k}'_\parallel} W^I_{i\mathbf{k}_\parallel,i'\mathbf{k}'_\parallel}. \quad (12)$$

The calculated results of $P^I_{i\mathbf{k}_\parallel}$ are shown in Fig. 3 as functions of the kinetic energy $\varepsilon_{\mathbf{k}_\parallel}$ for the alloy disorder scattering (curve *A*), for the acoustic phonon scattering due to deformation potential and piezoelectric interaction (curve *B*), for the $|i,\mathbf{k}\rangle$ to $|i+1,\mathbf{k}'\rangle$ LO phonon emission (curve *C*), and for the $|i,\mathbf{k}\rangle$ to $|i+2,\mathbf{k}'\rangle$ LO phonon emission (curve *D*). We notice

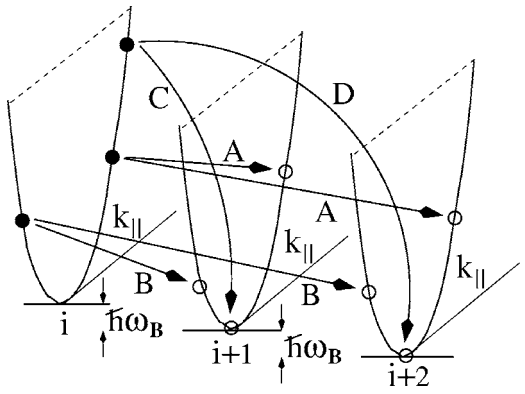

FIG. 4. The current-carrying electron transport processes in a SSL sample corresponding to the four scattering rates shown in Fig. 3.

that in Fig. 3 there are threshold energies in $\varepsilon_{\mathbf{k}_\parallel}$ for the LO phonon emission processes, but no threshold for the alloy disorder and the acoustic phonon scattering. To illustrate this difference more clearly, the corresponding electron transport processes within the SSL sample are illustrated in Fig. 4.

We see from Fig. 3 that the total scattering rate

$$P_{i\mathbf{k}_\parallel} = \sum_I P^I_{i\mathbf{k}_\parallel} \tag{13}$$

is dominated by the LO phonon emission processes, and by the interlevel transitions induced by the alloy disorder scattering with a change of the electron kinetic energy by an integer multiple of $\hbar\omega_B$. Such characteristic features will appear in the distribution function, and so have significant influence on the drift velocity to be presented in the next section.

IV. DRIFT VELOCITY

Using the Monte Carlo method to obtain the carrier drift velocity in a SSL under an applied electric field, we will first simulate the steady-state distribution function of the two-dimensional carriers belonging to any WSL level, since the distribution functions associated with different WSL levels are equivalent to each other. It is important to mention that in our Monte Carlo calculation of the distribution function, carriers can undergo scattering-assisted hops between different WSL levels. Without such hops included, the net drift velocity will be zero.

With the scattering rates given in the previous section, we use the standard Monte Carlo procedure[22] to keep track the motion of an electron starting from the initial state $|i\mathbf{k}_\parallel\rangle$. In this way we can derive the time $T(\mathbf{k}_\parallel)$ that an electron spends in the two-dimensional quantum state $|\mathbf{k}_\parallel\rangle$, which is the same for all WSL levels. This time is proportional to the two-dimensional electron distribution function $f(\mathbf{k}_\parallel)$, and hence we have $f(\mathbf{k}_\parallel)=AT(\mathbf{k}_\parallel)$. The normalization constant A is determined from the condition

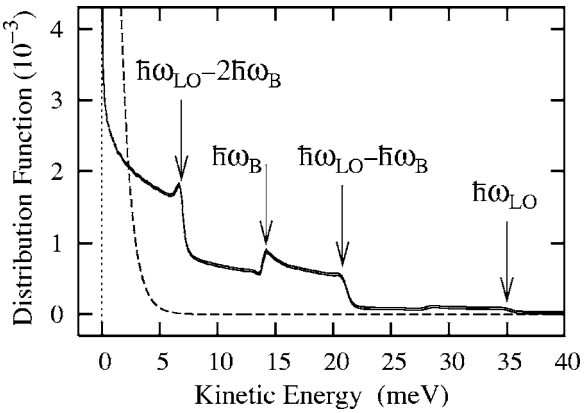

FIG. 5. The two-dimensional carrier distribution function $f(\mathbf{k}_\parallel)$ vs the two-dimensional kinetic energy $\varepsilon_{\mathbf{k}_\parallel}$ for an applied electric field $\mathcal{E}=16$ kV/cm. The corresponding Bloch oscillation energy $\hbar\omega_B=14.4$ meV. The calculation is performed at the temperature 10 K on the sample described in Sec. II. The threshold energies $\hbar\omega_{LO}-2\hbar\omega_B$, $\hbar\omega_{LO}-\hbar\omega_B$, and $\hbar\omega_{LO}$ for the LO phonon emission processes are indicated by arrows.

$$n = \frac{2}{V}\sum_{\mathbf{k}_\parallel} T(\mathbf{k}_\parallel), \tag{14}$$

where n is the two-dimensional electron concentration.

The Monte Carlo simulation was performed at the temperature 10 K on the sample described in Sec. II. The calculated $f(\mathbf{k}_\parallel)$ as a function of $\varepsilon_{\mathbf{k}_\parallel}$ for an electric field of 16 kV/cm is shown in Fig. 5 as the solid curve. The dashed curve in the same figure is the Fermi distribution function of the two-dimensional electron gas in the absence of an externally applied field. Because of the various scattering processes, especially the interlevel elastic scattering, which leads to the increase of the kinetic energy of carriers transferred into the neighboring wells, the tremendous broadening of the nonequilibrium distribution $f(\mathbf{k}_\parallel)$ from the Fermi function is expected. The kink at $\varepsilon_{\mathbf{k}_\parallel}=\hbar\omega_B=14.4$ meV in Fig. 5 is caused by the interlevel alloy disorder scattering (process A in Fig. 4) when the initial electron kinetic energy is close to zero. The distribution function exhibits sharp edges at $\varepsilon_{\mathbf{k}_\parallel}=\hbar\omega_{LO}-2\hbar\omega_B$, $\hbar\omega_{LO}-\hbar\omega_B$, and $\hbar\omega_{LO}$ due to the resonant LO phonon emission processes, which were discussed in connection to Figs. 3 and 4. Similar features appear in the semianalytical solution by Bryksin and Kleinert.[17]

When we perform the Monte Carlo simulation by tracking the motion of a carrier scattered by various mechanisms, we also track the position of the electron in the SSL since the interlevel scattering will move the electron from one unit cell of the SSL to another one. Therefore, we know the position of the electron as a function of time, and hence we can calculate the electron drift velocity.[23] The open-circle curve in Fig. 6 represents our calculated steady state velocity, at the temperature 10 K, as a function of the applied electric field. The solid curve is obtained using the Esaki-Tsu formula.[1] Using the dimensionless Esaki-Tsu smooth curve as a reference, it is clear that our calculated result exhibits the behavior of an oscillating negative differential velocity. A maxi-

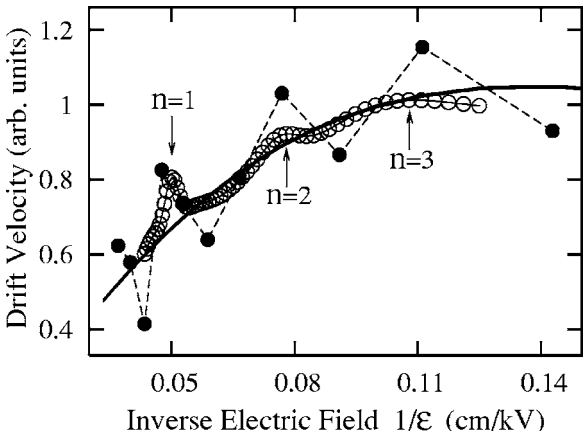

FIG. 6. The electric field dependence of the steady-state velocity obtained from Monte Carlo simulation (open-circle curve), and that extracted from the time-resolved measurements (Ref. 18) of THz response of a SSL on femtosecond optical pulse excitation (solid circles). The solid curve is the Esaki-Tsu result (Ref. 1). All data are for the sample described in Sec. II at the temperature 10 K.

mum of the oscillation occurs when the ratio $\hbar\omega_{LO}/\hbar\omega_B$ between the LO-phonon energy and the Bloch oscillation energy is an integer n, which is consistent with results of Bryksin and Kleinert.[17] In this case, by emitting a LO phonon, the electron has a large probability to hop a distance of nd, namely, n superlattice periods. The three maxima in Fig. 6 correspond to $\hbar\omega_{LO}/\hbar\omega_B=1$, 2, and 3. The amplitude of the maximum located at weaker fields decays due to the diminishing of overlap integrals in scattering matrix elements in Eq. (5).

V. TIME-RESOLVED THz MEASUREMENTS

A relevant experiment[18] was performed at the temperature 10 K on the same sample as described in Sec. II. This undoped SSL was grown on an n^+-GaAs (100) substrate by molecular beam epitaxy. The top and the bottom contacts were formed by depositing a semitransparent NiCr Schottky film and a AuGeNi/Au layer, respectively. By using these two electrodes, a static bias electric field $\mathcal{E}$ was applied to the undoped SSL region. In order to create carriers in the miniband, the sample was illuminated with femtosecond laser pulses from a tunable $Ti:Al_2O_3$ laser operated at a repetition frequency of 76 MHz. The spectral width of the laser pulses was 15 nm. The photoexcited carrier density was maintained below 1×10^{15} cm^3 in order to avoid field screening by photoexcited carriers. Since the holes are much heavier than the electrons, each hole is considered as localized in a quantum well. Therefore, under the driving force of the applied electric field, the emitted THz radiation is dominated by the accelerated electrons in the miniband and the electric field component E_{THz} of this radiation is proportional to the acceleration of photoexcited electrons. The emitted E_{THz} was detected in a reflection geometry by the free-space THz electro-optic sampling technique.[24] This sampling technique allows us to measure both the amplitude and the phase of the emitted THz radiation. The waveforms of E_{THz} measured at various acceleration fields are plotted in Fig. 7.

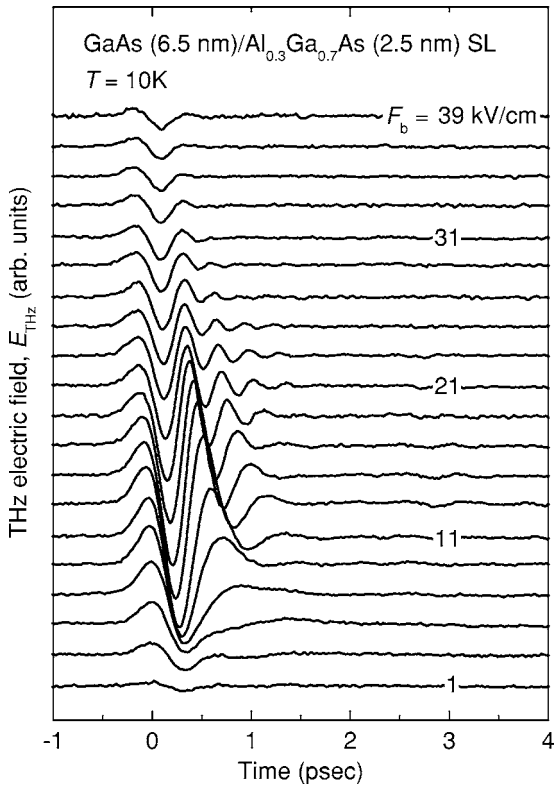

FIG. 7. The wave forms of the THz radiation emitted from the SL sample recorded for various bias electric fields $F(1-39$ kV/cm, 2 kV/cm step). The traces are shifted for clarity.

To obtain the velocity of the electrons under a specific field strength $\mathcal{E}$, the corresponding measured E_{THz} was integrated with respect to time.[18] The so-derived transient velocity is shown in Fig. 8. The steady-state velocity was obtained by plotting the velocity at 2 ps after the photoexcitation and

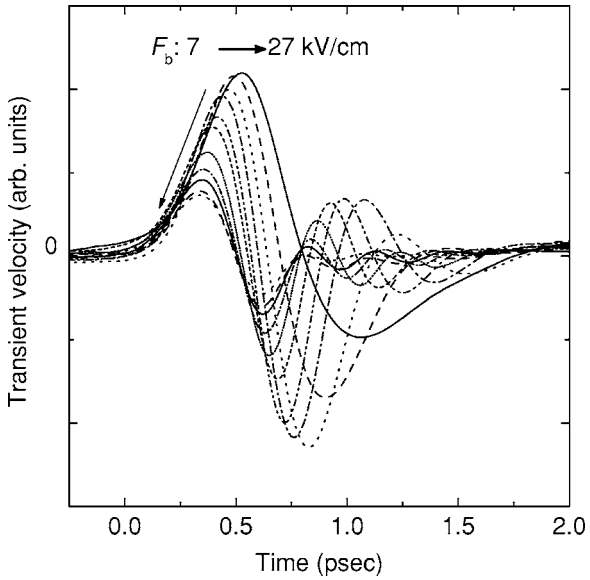

FIG. 8. The transient velocity obtained by integrating the measured THz wave forms. At 2 ps after the photoexcitation, the transient velocity settles down to the steady state.

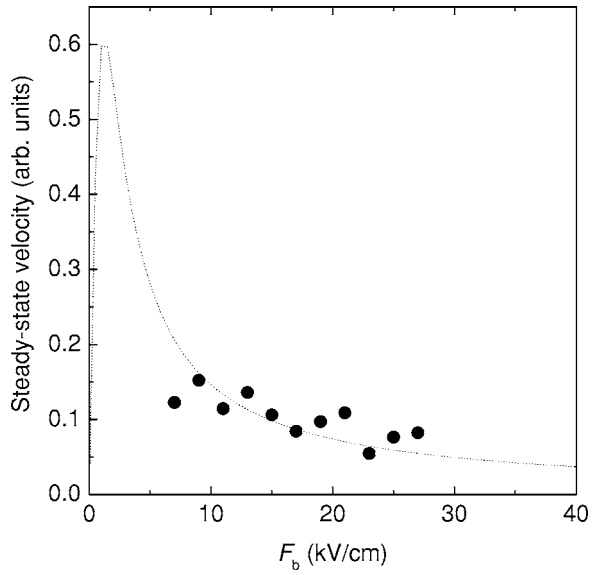

FIG. 9. The steady-state velocity vs acceleration field. Full circles are the experimental data. The dashed curve is the steady-state drift velocity calculated by semiclassical Esaki-Tsu theory.

plotted in Fig. 9 as a function of the applied electric field, together with the steady-state velocity predicted by a semiclassical Esaki-Tsu theory.[1] In the calculation, we set the scattering time to be 0.63 ps [the geometrical mean of the momentum-relaxation time (0.2 ps) and the energy-relaxation time[18] (2 ps)]. The experimentally obtained steady-state velocity was replotted by solid circles in Fig. 6 as a function of $1/\mathcal{E}$ (notice that in both Fig. 9 and Fig. 6 the velocity is in arbitrary units). The experimentally obtained dimensionless drift velocity exhibits oscillations with maxima located at the electric field values, where the peaks originating from electron-phonon resonances are present in our calculated open-circle curve.

VI. CONCLUSIONS

We have performed a refined Monte Carlo study on the electron transport in AlGaAs/GaAs superlattices under the applied electric field strength corresponding to the localized WSL regime. The electron transport is induced by scattering-assisted electron hops between different WSL levels. Contribution of various scattering mechanisms to the total scattering probability is analyzed.

We found that the elastic alloy disorder scattering in this type of SL leads to a significant broadening of the in-plane distribution function, and that the LO phonon emission processes provide the essential resonant transfer of an electron from the ith WSL level to the $(i+1)$th and the $(i+2)$th WSL levels. These processes lead to peaks in the negative differential velocity behavior when the electric field strength satisfies the condition that the ratio $\hbar\omega_{LO}/\hbar\omega_B$ is an integer. This condition also manifests itself in the calculated two-dimensional electron distribution function: a threshold edge appears when the two-dimensional electron kinetic energy $\varepsilon_{\mathbf{k}_\parallel}$ is equal to $\hbar\omega_{LO}-n\hbar\omega_B \geqslant 0$, where n is a non-negative integer.

A technique for experimental determination of the electron drift velocity in SSL on the basis of data measured with THz time-resolved spectroscopy was presented. The theoretically calculated oscillating behavior of the negative differential velocity was also found in the experimentally determined electron drift velocity. This agreement supports the present theory and the earlier analytical model[17] of scattering-assisted electric current in SSL in the Wannier-Stark regime.

ACKNOWLEDGMENTS

This work was supported by grants from the Nordic Research Board, the Russian Foundation for Basic Research, the Russian Academy of Science, and the Russian Ministry of Science.

[1] L. Esaki and R. Tsu, IBM J. Res. Dev. **14**, 61 (1970).
[2] J. Feldmann, K. Leo, J. Shah, D. A. B. Miller, J. E. Cunningham, T. Meier, G. von Plessen, A. Schulze, P. Thomas, and S. Schmitt-Rink, Phys. Rev. B **46**, R7252 (1992).
[3] C. Waschke, H. G. Roskos, R. Schwedler, K. Leo, H. Kurz, and K. Köhler, Phys. Rev. Lett. **70**, 3319 (1993).
[4] T. Dekorsy, P. Leisching, K. Köhler, and H. Kurz, Phys. Rev. B **50**, R8106 (1994).
[5] F. Löser, Yu. A. Kosevich, K. Köhler, and K. Leo, Phys. Rev. B **61**, R13373 (2000).
[6] Y. Shimada, K. Hirakawa, and S.-W. Lee, Appl. Phys. Lett. **81**, 1642 (2002).
[7] S. A. Ktitorov, G. S. Simin, and V. Y. Sindalovskii, Fiz. Tverd. Tela (Leningrad) **13**, 2230 (1971) [Sov. Phys. Solid State **13**, 1872 (1971)].
[8] L. K. Orlov and Yu. A. Romanov, Fiz. Tverd. Tela (Leningrad) **19**, 726 (1997) [Sov. Phys. Solid State **19**, 421 (1977)].
[9] Yu. A. Romanov, V. Bovin, and L. Orlov, Fiz. Tekh. Poluprovodn. (S.-Peterburg) **12**, 1665 (1978) [Sov. Phys. Semicond. **12**, 987 (1978)].
[10] A. A. Ignatov, K. F. Renk, and E. P. Dodin, Phys. Rev. Lett. **70**, 1996 (1993).
[11] H. Kroemer, cond-mat/0007482 (unpublished).
[12] A. Wacker and A.-P. Jauho, Phys. Rev. Lett. **80**, 369 (1998); A. Wacker, A.-P. Jauho, S. Rott, A. Markus, P. Binder, and G. H. Döhler, *ibid.* **83**, 836 (1999); A. Wacker, Phys. Rev. B **66**, 085326 (2002).
[13] D. L. Andersen and E. J. Aas, J. Appl. Phys. **44**, 3721 (1973); R. K. Reich, R. O. Grondin, and D. K. Ferry, Phys. Rev. B **27**, 3483 (1983); M. Artaki and K. Hess, Superlattices Microstruct. **1**, 489 (1985).
[14] E. Schomburg, N. V. Demarina, and K. F. Renk, Phys. Rev. B **67**, 155302 (2003).
[15] G. H. Wannier, Rev. Mod. Phys. **34**, 645 (1962).
[16] R. Tsu and G. Döhler, Phys. Rev. B **12**, 680 (1975).
[17] V. V. Bryksin and P. Kleinert, J. Phys.: Condens. Matter **9**, 7403

(1997).
[18] N. Sekine and K. Hirakawa, Phys. Rev. Lett. **94**, 057408 (2005).
[19] Kuijuan Jin, M. Odnoblyudov, Y. Shimada, K. Hirakawa, and K. A. Chao, Phys. Rev. B **68**, 153315 (2003).
[20] L. W. Wang, A. Zunger, and K. A. Mader, Phys. Rev. B **53**, 2010 (1996).
[21] P. Ray and P. K. Basu, Phys. Rev. B **45**, 9169 (1992).
[22] C. Jacoboni and L. Reggiani, Rev. Mod. Phys. **55**, 645 (1983).
[23] P. M. Richards, Phys. Rev. B **16**, 1393 (1977).
[24] Q. Wu and X.-C. Zhang, Appl. Phys. Lett. **71**, 1285 (1997); A. Leitenstorfer, S. Hunsche, J. Shah, M. C. Nuss, and W. H. Knox, *ibid.* **74**, 1516 (1999).